# Multifunctional Biocompatible Graphene Oxide Quantum Dots Decorated Magnetic Nanoplatform for Efficient Capture and Two-Photon Imaging of Rare Tumor Cells

Yongliang Shi,[†] Avijit Pramanik,[†] Christine Tchounwou,[†] Francisco Pedraza,[‡] Rebecca A. Crouch,[†] Suhash Reddy Chavva,[†] Aruna Vangara,[†] Sudarson Sekhar Sinha,[†] Stacy Jones,[†] Dhiraj Sardar,[‡] Craig Hawker,[§] and Paresh Chandra Ray*,[†]

[†]Department of Chemistry and Biochemistry, Jackson State University, Jackson, Mississippi 39217, United States

[‡]Department of Physics and Astronomy, University of Texas at San Antonio, San Antonio, Texas 78249, United States

[§]Department of Chemistry and Biochemistry and Materials Research Laboratory, Materials Department, University of California at Santa Barbara, Santa Barbara, California 93106, United States

**ABSTRACT:** Circulating tumor cells (CTCs) are extremely rare cells in blood containing billions of other cells. The selective capture and identification of rare cells with sufficient sensitivity is a real challenge. Driven by this need, this manuscript reports the development of a multifunctional biocompatible graphene oxide quantum dots (GOQDs) coated, high-luminescence magnetic nanoplatform for the selective separation and diagnosis of Glypican-3 (GPC3)-expressed Hep G2 liver cancer tumor CTCs from infected blood. Experimental data show that an anti-GPC3-antibody-attached multifunctional nanoplatform can be used for selective Hep G2 hepatocellular carcinoma tumor cell separation from infected blood containing 10 tumor cells/mL of blood in a 15 mL sample. Reported data indicate that, because of an extremely high two-photon absorption cross section (40530 GM), an anti-GPC3-antibody-attached GOQDs-coated magnetic nanoplatform can be used as a two-photon luminescence platform for selective and very bright imaging of a Hep G2 tumor cell in a biological transparency window using 960 nm light. Experimental results with nontargeted GPC3(−) and SK-BR-3 breast cancer cells show that multifunctional-nanoplatform-based cell separation, followed by two-photon imaging, is highly selective for Hep G2 hepatocellular carcinoma tumor cells.

**KEYWORDS:** luminescent magnetic nanoplatform, graphene oxide quantum dots, highly efficient two-photon-absorbing material, rare liver cancer cell separation from blood, selective two-photon imaging
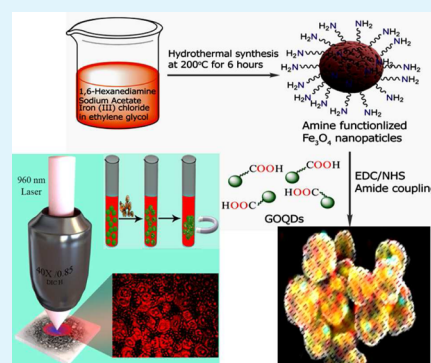
## 1. INTRODUCTION

Liver cancer is the third leading cause of cancer-related deaths worldwide.[1,2] During the past few years, several clinical studies have demonstrated that HCC tumor circulating tumor cells (CTCs) can be used as a marker for understanding metastatic development, which is a key for the overall survival of liver cancer.[2−6] The selective capture and accurate analysis of hepatocellular carcinoma (HCC) tumor CTCs from a blood sample can be a very powerful noninvasive approach for the early detection of liver cancer. Because CTCs are extremely rare malignant cells in blood containing billions of red blood cells for liver cancer patients, until now capturing and accurately identifying CTCs has been highly challenging.[7−16] Clinical practitioners need highly sensitive and specific methods to detect early stage CTCs to be used as a liquid bioassay for early stages of liver cancer while surgery may still be effective.[3−6] Driven by this need, in this manuscript, we report the development of multifunctional graphene oxide quantum dots (GOQDs)-coated, high-fluorescence magnetic nanoplatforms, which have exciting potential for improving HCC cancer diagnosis by selectively separating and detecting liver cancer

tumor CTCs from infected blood using multiphoton luminescence. In our design, we have combined multiple discrete components, such as GOQDs and magnetic nanoplatforms, into a single and compact multifunctional nanoplatform, as shown in Scheme 1, which will have a profound impact on rare cell separation and capture from a whole blood sample as well as molecular diagnostics via two-photon imaging.
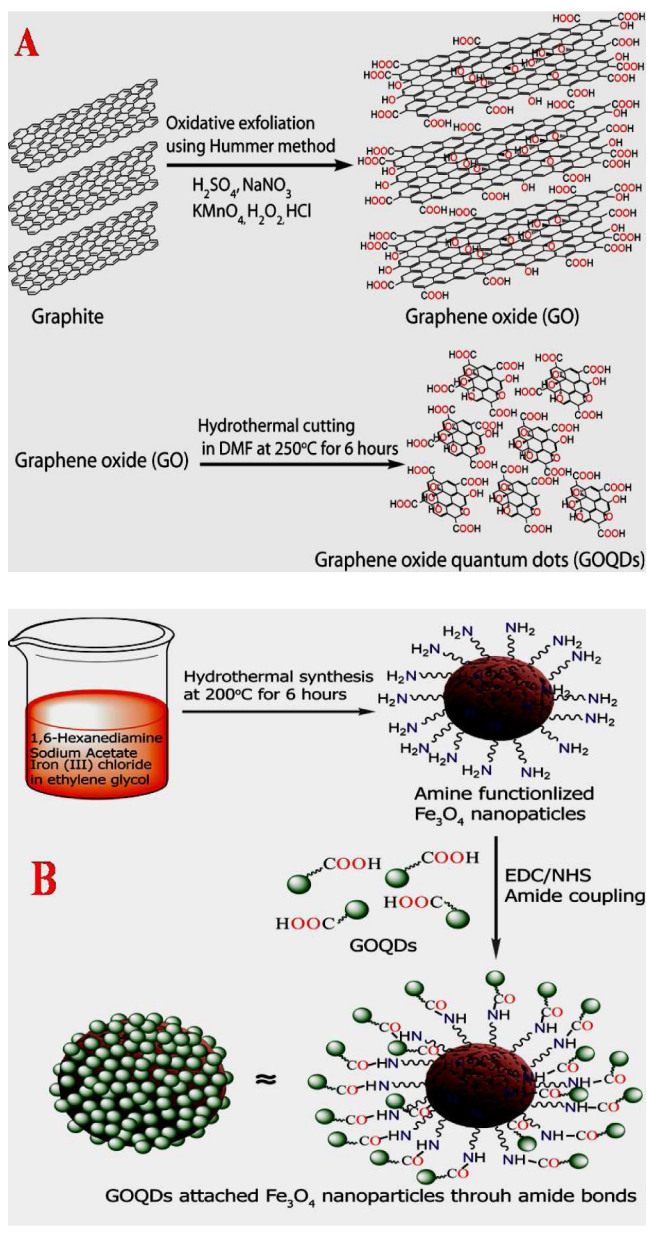
Because of the natural fact that all untreated biological materials are diamagnetic,[7−16] magnetic cell separation is thought to be highly specific and can be applied to separate CTCs from whole blood. As a result, in our design, magnetic nanoplatforms are used to capture and separate HCC tumor cells from whole blood by using a bar magnet, as shown in Scheme 2A. This process also allowed us to avoid huge light scattering and autofluorescence background from blood cells.[7−16] On the other hand, photoluminescence from GOQDs has been used for the accurate identification of
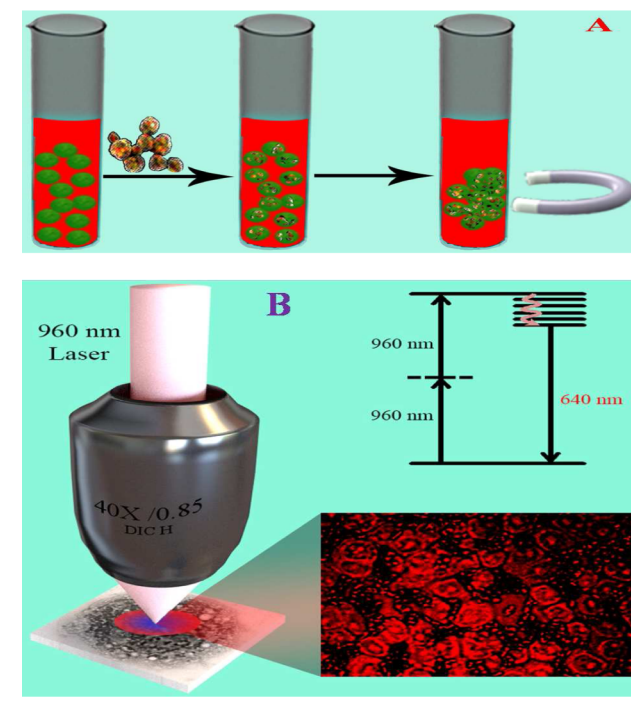
**Scheme 1. Schematic Representations Showing the Synthetic Procedure for the Development of (A) GOQDs and (B) GOQDs-Coated High-Fluorescence Magnetic Nanoplatforms**



**Scheme 2. Schematic Representation Showing (A) Magnetic Selective Separation of Hep G2 Tumor Cells from a Whole Blood Sample Using a GPC3-Specific Monoclonal Anti-GPC3-Antibody-Attached GOQDs-Coated Magnetic Nanoplatform and (B) TPL Imaging of Hep G2 Tumor Cells Using 960 nm Light after Magnetic Separation**



nm provides a maximum radiation penetration through tissue, we have to use GOQDs-based two-photon imaging.[21,22,40,42,43] High two-photon absorption cross sections, biocompatibility, and long-time photostability are the main factors that govern whether two-photon fluorescent imaging materials[40−43] can be used for cancer imaging or not. As a result, here we report that, because of a very high two-photon absorption cross section, our developed GOQDs-coated magentic nanoplatform has good biocompatibility and photostability and is highly suitable for label-free bright two-photon imaging of HCC tumor cells after separation from whole blood. Because GOQDs contain different carbon- and oxygen-containing moieties at the edge, as shown in Scheme 2, we have used those groups for subsequent functionalization with a monoclonal anti-Glypican-3 (GPC3) antibody for the selective capture, separation, and imaging of HCC tumor cells from whole blood. It is now well documented that GPC3 is significantly overexpressed in the human HCC cell line Hep G2.[3−6] As a result, for selective capture and accurate analysis, we have designed a versatile platform using a GPC3-specific monoclonal anti-GPC3-anti-body-attached GOQDs-coated magnetic nanoplatform. Using GPC3(−) normal skin HaCaT and breast cancer SK-BR-3 cells, we have demonstrated that GOQDs-coated magnetic-nano-platform-based assay has the capability of enabling distinction from nontargeted cell lines.

## 2. EXPERIMENTAL SECTION

**2.1. Materials.** Monoclonal anti-GPC3 antibody, graphite, sodium nitrate, sulfuric acid, hydrochloric acid, potassium permanganate, a 30% hydrogen peroxide solution, iron(III) chloride, tetramethylam-monium hydroxide, and poly(ethylene glycol) (PEG; average $M_n =$ 400) were purchased from Sigma-Aldrich (St. Louis, MO). The human

HCC tumor cells using multiphoton luminescence, as shown in Scheme 2B. Nanometer-sized graphene oxide, known as GOQDs, exhibits novel properties because of quantum confinement.[17−25] When 2-dimensional graphene oxide sheets are converted into 0-dimensional chemically stable GOQDs, wonderful photoluminescence and optoelectronic properties can be obtained because of strong quantum confinement and edge effects.[26−35] Because of their very easy and low-cost large-scale production as well as remarkable properties, GOQDs hold great promise for daily life applications.[36−42]

Reported experimental data from different groups have demonstrated that GOQDs photoluminescence can be tuned from 400 to 600 nm. As a result, GOQDs are not suitable for single-photon biological imaging using near-infrared (NIR) light within a biological transparency window.[30,32,33,38−41] Because NIR biological window light between 700 and 1350
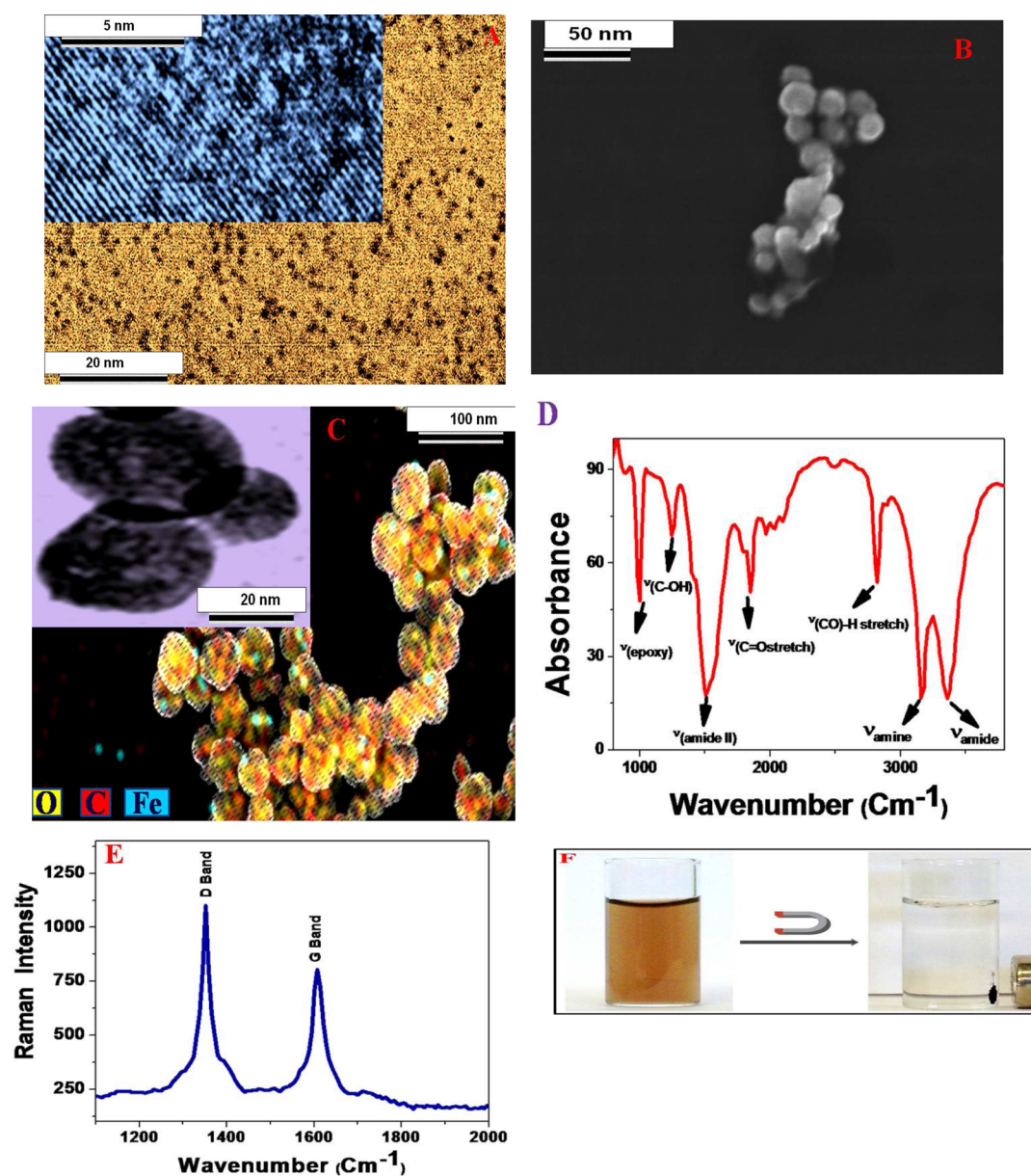
**Figure 1.** (A) TEM image showing the morphology of GOQDs. Inset: HRTEM image showing the high crystallinity of the developed GOQDs. (B) High-resolution SEM image showing the morphology of magnetic nanoparticles. (C) High-resolution SEM image showing the morphology of GOQDs-coated magnetic nanoplatforms. The EDX mapping shows the presence of Fe, C, and O in GOQDs-coated magnetic nanoplatforms. Inset: HRTEM image, which indicates the presence of GOQDs on the surface of the magnetic nanoplatform. (D) FTIR spectra from GOQDs-coated magnetic nanoplatforms verifying the existence of hydrogen bonding, −CONH, −NH, −C═O, −COH, epoxy group, etc. (E) Raman spectrum clearly showing the presence of D and G bands. Strong D bands clearly indicate the high defect due to the presence of magnetic nanoplatforms. (F) Photograph demonstrating that GOQDs-coated magnetic nanoplatforms is highly magnetic, and as a result, we can separate them by using a bar magnet.

HCC cell lines, Hep G2, were purchased from the American Type Culture Collection (ATCC, Rockville, MD). Whole rabbit blood was purchased from Colorado Serum Company (Denver, CO).

**2.2. Synthesis of GOQDs.** GOQDs-decorated, highly photoluminescent magnetic nanoplatforms were synthesized using a multistep process, as shown in Scheme 1. Initially, graphene oxide (GO) was prepared by a modified Hummers method,[19] as previously reported,[21,22] using a natural graphite powder with an average size of 150 $\mu$m. Next, GOQDs were prepared from GO, as shown in Scheme 2A. A total of 0.15 g of freshly synthesized GO was treated with 30 mL of N,N-dimethylformamide (DMF) and heated at 250 °C for 6 h. After heating, the reaction mixture was vacuum-filtered using a 0.2 $\mu$m nylon membrane. Solid GOQDs were obtained by evaporating the solvent from the filtrate using a rotary evaporator. Figure 1A shows the

transmission electron microscopy (TEM) image of freshly prepared GOQDs. The inserted figure in Figure 1A shows the high-resolution TEM (HRTEM) images and indicates the high crystallinity of the GOQDs, with lattice spacing around 0.32 nm, which is quite near the 0.32 nm interlayer spacing of bulk graphite.

**2.3. Synthesis of Amine-Functionalized Magnetic Nanoparticles.** The amine-functionalized magnetic nanoparticles were prepared from ferric chloride, as shown in Scheme 1B. A total of 0.51 g of FeCl$_3$·6H$_2$O (1.89 mmol), 2.0 g of NaOAc (48.78 mmol), and 1.8 g of 1,6-hexadiamine (30.98 mmol) were dissolved in 15 mL of ethylene glycol ($d$ = 1.11 g/mL). The solution was transferred into an autoclave, incubated at 200 °C for 6 h, and cooled to room temperature. The reaction mixture was centrifuged at 14000 rpm for 5 min to remove the ethylene glycol. Then the obtained residue was

redispersed in 15 mL of nanopure water. The brown suspension was centrifuged again at 14000 rpm for 5 min. After that, the aqueous supernatant was removed and 145 mL of nanopure water was added. The colloid solution was stored at room temperature for future use. After that, magnetic nanoparticles were characterized using high-resolution scanning electron microscopy (SEM). The SEM image in Figure 1B shows that the average particle size is about 25 nm. Because it is well-known that TEM/SEM grid preparation can increase aggregation, as we have noted in our SEM image reported in Figure 1B, we have also performed dynamic light scattering (DLS) measurement using a Malvern Zetasizer Nano instrument in solution phase. Both DLS and SEM data, as reported in Table 1, indicate that

**Table 1. Average Particle Size (nm) Measured by DLS and SEM**

| nanoparticle description | size measured by DLS | size measured by SEM |
|---|---|---|
| magnetic nanoparticle | 26 ± 4 | 25 ± 4 |
| magnetic-nanoparticle-attached GOQDs | 38 ± 5 | 40 ± 5 |

the average size is about 25 nm for magnetic nanoparticles. The magnetic properties determined using a superconducting quantum interference device (SQUID) magnetometer at room temperature indicate superparamagnetic behavior with a specific saturation magnetization of 46.3 emu/g for the amine-functionalized magnetic nanoparticle.

## 2.4. Synthesis of a Multifunctional GOQDs-Coated Magnetic Nanoplatform.

GOQDs oxygen-containing functional groups serve as anchoring points for the development of a GOQDs-coated high-fluorescence magnetic nanoplatform. To accomplish this we used coupling chemistry between a $-CO_2H$ group of the GOQDs and a $-NH_2$ group of the amine-functionalized magnetic nanoplatform via amide linkages, as shown in Scheme 1B. A total of 6.05 mg of GOQDs was dissolved in 3 mL of 2-($N$-morpholino)ethanesulfonic acid buffer. A total of 2 mL of 2 mg/mL $N$-hydroxysuccinimide was added to the GOQDs solution. After vortexing, 1 mL of 2 mg/mL 1-[3-(dimethylamino)propyl]-3-ethylcarbodiimide hydrochloride was added to the reaction mixture. After 20 min, 5 mL of a $Fe_3O_4-NH_2-C_6H_{12}-NH_2$ nanoplatform was added dropwise with constant shaking. The mixture was sonicated for 4 h, kept overnight under shaking, and then dialyzed overnight in a 2000 Da MWCO dialysis tube. After that, the reaction product was dissolved in 50 mL of water, and we used a magnet to separate GOQDs-coated magnetic nanoparticles from unreacted GOQDs. The purified particles were characterized by various spectroscopic techniques. Fourier transform infrared spectroscopy (FTIR), Raman spectroscopy, and high-resolution SEM were used to characterize the membrane, as reported in Figure 1. The SEM and inset HRTEM image, as shown in Figure 1C, show that the size is about 40 nm for the magnetic nanoplatform, which is about 15 nm more than only the magnetic nanoparticle. Because it is well-known that TEM/SEM grid preparation can increase aggregation, as we have noted in our SEM image reported in Figure 1C, we have also performed DLS measurement in solution phase. Both DLS and SEM data, as reported in Table 1, indicate that the average size is about 40 nm for GOQDs-conjugated magnetic nanoparticles.
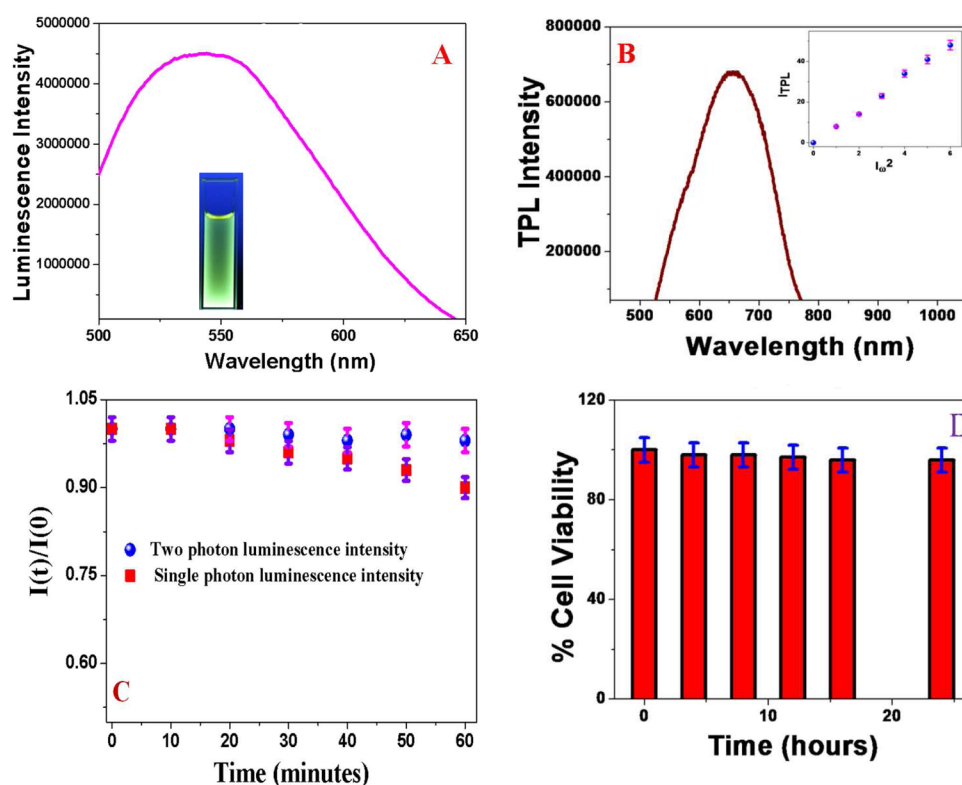


**Figure 2.** (A) Single-photon photoluminescence from a freshly prepared GPC3-specific monoclonal anti-GPC3-antibody-attached GOQDs-coated magnetic nanoplatform. We have used 440 nm for the excitation. Inset: Photograph showing the luminescence from a multifunctional nanoplatform in the presence of UV light. (B) Two-photon photoluminescence spectra from an anti-GPC3-antibody-attached GOQDs-coated magnetic nanoplatform, when the multifunctional nanoplatform was excited using 960 nm light. Inset: Plot demonstrating how the photoluminescence at 640 nm varies with the square of the intensity of 960 nm excitation. The linear plot indeed indicates that the observed luminescence is TPL. (C) Plot showing the photostability of an anti-GPC3-antibody-attached fluorescence magnetic nanoplatform. Our data clearly show that the stability for the TPL intensity is better than that of single-photon luminescence. (D) Plot demonstrating the biocompatibility of an anti-GPC3-antibody-attached GOQDs-coated magnetic nanoplatform against HCC cancer cells. Even after 24 h of incubation, we observed about 96% cell viability.

The FTIR spectrum of the GOQDs-coated magnetic nanoplatform, as shown in Figure 1E, exhibits a very strong and broad band between ~3100 and 3450 cm$^{-1}$, which is due to the amide I band and the N−H stretching vibration for the amine-functionalized nanoplatform and the −OH vibration from GOQDs carboxyl groups. The carbonyl (−C═O) stretch observed at ~1725 cm$^{-1}$ and the (CO)−H stretch at ~2720 cm$^{-1}$ correspond to unreacted carboxylic acid groups of GOQDs.

The amide II band observed at ~1550 cm$^{-1}$ is mainly due to the in-plane NH bending vibration of the amide group. Similarly, we have observed an unreacted epoxy group vibration at ~975 cm$^{-1}$. The Raman spectrum from the GOQDs-coated magnetic nanoplatform, as shown in Figure 1E, clearly indicates a very strong D band at ~1340 cm$^{-1}$ and a G band at ~1620 cm$^{-1}$, which indicate that GOQDs are coated on the magnetic nanoplatform.[11−20] The strong D band indicates that the degree of graphene modification is high. The high-resolution SEM with EDX imaging, as shown in Figure1C, confirms the presence of Fe, C, and O in the GOQDs-coated magnetic nanoplatform. The inset HRTEM image in Figure 1C indicates the presence of GOQDs on the surface of the magnetic nanoplatform. SQUID magnetometry property measurement indicates superparamagnetic behavior with a specific saturation magnetization of 37.8 emu/g for the GOQDs-coated magnetite nanoplatforms. As a result, we are able to separate them by a bar magnet, as shown in Figure 1F.

**2.5. Preparation of a Monoclonal Anti-GPC3-Antibody-Conjugated Nanoplatform.** For the targeted capture and imaging of Hep G2 tumor cells, we have modified multifunctional nanoplatforms with a GPC3-specific monoclonal anti-GPC3 antibody, which is known to be specific to HCC tumor cells. To accomplish this, GOQDs-coated magnetic nanoplatforms were coated with amine-modified PEG (HS-PEG) to prevent nonspecific interactions with blood cells and cell media. After PEGylation, a GPC3-specific monoclonal anti-GPC3 antibody was attached to the amine-functionalized PEG-coated GOQDs-attached magnetic nanoplatform, as previously reported.[21,22,43]

**2.6. Two-Photon Luminescence (TPL) Measurement.** For two-photon fluorescence, we have used a 80 MHz Ti sapphire laser as an excitation source with a 100 fs pulse width and a 80 MHz repetition rate. 960 nm light was generated using an optical parametric amplifier. TPL spectra were recorded with a CCD camera after passing through a monochromator.

**2.7. Cell Culture and Incubation with Multifunctional GOQDs-Coated Magnetic Nanoplatforms.** Human HCC cell lines, Hep G2 tumor cells, were purchased from the American Type Culture Collection (ATCC) and grown according to the ATCC procedure. Briefly, cells were grown in a 5% CO$_2$ incubator at 37 °C using an Eagle's minimum essential medium and a Dulbecco's modified essential medium, which is supplemented with 10% premium fetal bovine serum and 100 units/mL penicillin/streptomycin in 75 cm$^2$ tissue culture flasks. Once the culture was 10$^5$ cells/mL, different numbers of HCC tumor cells were spiked in citrated whole rabbit blood at various densities. Next, different concentrations of anti-GPC3-antibody-attached multifunctional GOQDs-coated magnetic nanoplatforms were mixed with infected blood for 30 min at room temperature before the magnetic separation experiment was performed. After magnetic separation, we performed TEM and two-photon fluorescence analyses.

**2.8. Two-Photon Fluorescence Imaging Analysis.** For two-photon imaging at 960 nm light, we used a Nikon multiphoton microscope (FV1000MPE), as shown in Scheme 1. Details were reported previously.[21,22,43] For two-photon imaging, we used a 80 MHz Ti sapphire laser as an excitation source with a 100 fs pulse width and a 80 MHz repetition rate. 960 nm light in a biological transparency window was generated using an optical parametric amplifier.

**2.9. Enzyme-Linked Immunosorbent Assay Analysis.** The amount of GPC3 levels in the captured cell was measured using the ELISA kit in accordance with the manufacturer's instructions. We purchased these kits from USCN Life Science Inc.

## 3. RESULTS AND DISCUSSION

Figure 2A shows the single-photon luminescence spectra at 440 nm excitation from GPC3-specific monoclonal anti-GPC3-antibody-attached GOQDs-coated magnetic nanoplatforms. In GOQDs, the aromatic sp$^2$ domains are surrounded by a carboxyl-, epoxy-, and hydroxyl-bound sp$^3$ matrix.[30,32,33,38−41] As a result, the GOQDs luminescence property will be determined by the $\pi$ and $\pi^*$ electronic levels of the sp$^2$ aromatic structures, as well as by the band gap of the $\sigma$ and $\sigma^*$ states of the sp$^3$ matrix.[30,32,33,38−41] Reported single-photon TPL data show that the multifunctional nanoplatform is not suitable for human cancer imaging applications using the biological transparency windows. To overcome this, we have employed TPL imaging using 960 nm excitation light. The two-photon photoluminescence spectra from the antibody-attached GOQDs-coated magnetic nanoplatform, as shown in Figure 2B, shows a quite bright luminescence maximum around 640 nm.

Next, to determine whether the observed luminescence from multifunctional nanoplatform was induced by two-photon excitation, we have performed 960 nm excitation wavelength power dependent two-photon intensity measurements. The inserted figure in Figure 2B shows how 640 nm two-photon emission intensities varies with 960 nm laser excitation average powers. Experimental data indicate that the observed luminescence intensity is proportional to the square of the 960 nm excitation intensity, which indeed confirms the two-photon excitation process.

To determine the two-photon cross sections and fluorescence quantum yields of freshly prepared multifunctional magnetic nanoplatforms, we used rhodamine B (RhB), whose two-photon cross section and quantum yield are well documented, as a reference. By measuring the TPL intensity from multifunctional magnetic nanoplatforms and RhB, we determined the luminescence quantum yield for a freshly prepared anti-GPC3-antibody-attached GOQDs-coated magnetic nanoplatform as 0.32. The two-photon absorption cross-sectional values were obtained using the equation[32,33,38−41]

$$\sigma_{2D'GOQDs} = \sigma_{2D'RhB}\,(L_{GOQDs}/L_{RhB})(\Phi_{L'RhB}/\Phi_{L,GOQDs})$$
$$(C_{RhB}/C_{GOQDs}) \tag{1}$$

where the two-photon absorption cross section has been denoted as $\sigma_{2p}$ and the emission quantum yield has been denoted as $\Phi_L$. In eq 1, $L$ is the observed luminescence intensity and $C$ is the concentration used for the TPL experiments. Using eq 1 and RhB as the reference, we determined the two-photon absorption cross section for a freshly prepared anti-GPC3-antibody-attached GOQDs-coated magnetic nanoplatform as 40530 Goeppert−Mayer (GM) units (where 1 GM = 10$^{-50}$ cm$^4$·s/photon), at 960 nm excitation, which is 3 orders magnitude higher than the measured $\sigma_{2PA}$ for RhB (28 GM). The observed very high $\sigma_{2PA}$ for the multifunctional nanoplatform can be due to highly efficient intramolecular charge transfer between large $\pi$-conjugated systems of water-soluble GOQDs and the strong electron-donating carboxyl, hydroxyl, and amine groups. This strong intramolecular charge transfer enhances the two-photon absorption cross sections significantly.

Because it is well documented[27−40] that photobleaching of fluorophores via photodamage causes challenges in single-photon imaging experiments, the use of two-photon NIR excitation, as we have performed here, will minimize the
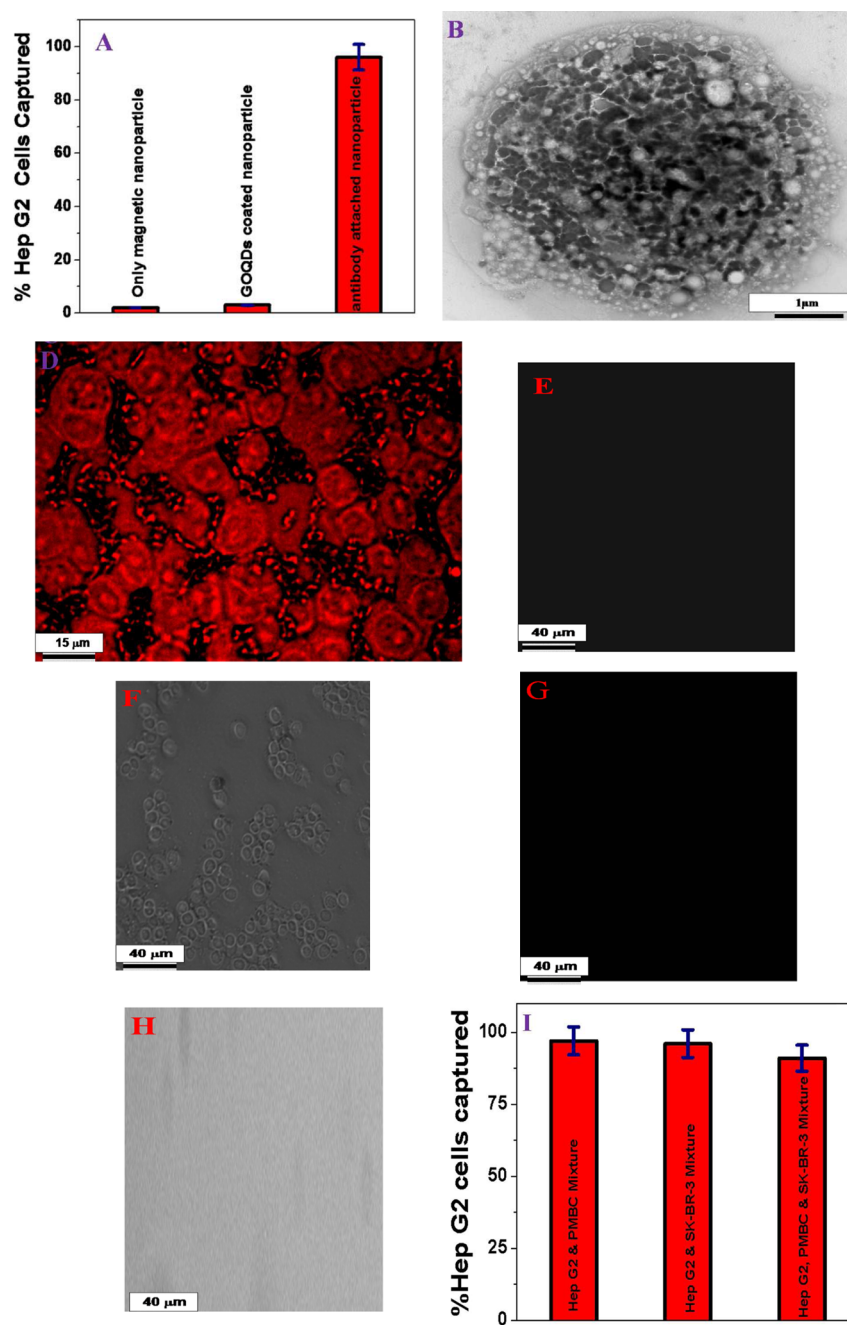
**Figure 3.** (A) ELISA results showing the Hep G2 tumor cell capture efficiency from an infected blood sample using the anti-GPC3-antibody-attached GOQDs-coated magnetic nanoplatform. Plots also show that the separation efficiency is less than 2% in the absence of an anti-GPC3 antibody. (B) TEM image showing that Hep G2 tumor cells are captured by the anti-GPC3-antibody-attached GOQDs-coated magnetic nanoplatform. Black materials on the cancer cells are the nanoplatform. Nanoplatforms are attached on the surface of the cancer cells via an antigen−antibody interaction. (C) TEM image of the Hep G2 tumor cells in the absence of the magnetic nanoplatform. (D) TPL image of the Hep G2 tumor cells after capture by the anti-GPC3-antibody-attached GOQDs-coated magnetic nanoplatform. We have used 960 nm light as the excitation source. (E) TPL image of a supernatant after magnet separation, which clearly shows that the anti-GPC3-antibody-attached GOQDs-coated magnetic nanoplatform does not bind with the blood cells. (F) Bright-field image of supernatant blood cells after magnetic separation. (G) Fluorescence image showing that the anti-GPC3-antibody-attached GOQDs-coated magnetic nanoplatform does not bind with GPC3(−)−SK-BR-3 breast tumor cells; as a result, the HaCaT cells were not separated by a magnet from the infected blood sample. (H) Bright-field image also indicating that no cells are separated during magnetic separation. (I) Percentage of Hep G2 positive cells captured by the anti-GPC3-antibody-attached GOQDs-coated magnetic nanoplatform, when citrated whole rabbit blood infected by 10 cells/mL Hep G2 tumor cells and $10^5$ cells/mL normal SK-BR-3 cells and PBMC cells each, respectively.

possible photodamage of the luminescence imaging material. To understand the photostability of the multifunctional magnetic nanoplatform, we performed time-dependent single-photon and two-photon intensity change experiments. As

shown in Figure 2C, TPL signals remain almost unchanged even after 1 h of illumination, which clearly indicates very the good photostability of the multifunctional magnetic nanoplatform as a TPL material. On the other hand, as shown in Figure

2C, the single-photon luminescence signal decreases by about 10% after 1 h of illumination, which clearly indicates that the photostability is better as a TPL material than as a single-photon luminescence material. To find the biocompatibility, which is very important for any material used for cell separation and imaging, anti-GPC3-antibody-attached GOQDs-coated magnetic nanoplatforms were incubated with $1.2 \times 10^5$ cells/mL of Hep G2 cancer cells for different time intervals less than or equal to 24 h. After incubation, the cell viability was measured using MTT testing.[21,22,43] Figure 2D clearly shows that, even after 24 h of incubation with Hep G2 cancer cells, 96% cell viability was observed. This clearly indicates a very good biocompatibility of our developed multifunctional magnetic nanoplatforms. We have also performed the same cell viability experiment with normal skin HaCaT cells and found more than 98% cell viability even after 24 h of incubation.

To demonstrate that the anti-GPC3-antibody-attached GOQDs-coated magnetic nanoplatform can be used for liver cancer CTC analysis close to clinical settings, we tested the selective capture and two-photon imaging capability using infected blood, as shown in Scheme 1. A 300 $\mu$L anti-GPC3-antibody-attached GOQDs-coated magnetic nanoplatform was incubated with infected blood containing $1.2 \times 10^3$ Hep G2 tumor cells in 15 mL suspensions of citrated whole rabbit blood for 90 min with gentle shaking. Next, a bar magnet was used to separate the Hep G2 tumor cells attached GOQDs-coated magnetic nanoplatform from the infected blood sample, as shown in Scheme 1. To determine the capture efficiency, we used an enzyme-linked immunosorbent assay (ELISA).

Our ELISA experimental results, as shown in Figure 3A, clearly indicate that the Hep G2 tumor cell separation efficiency is less than 2% when we have not attached anti-GPC3 antibody either with the magnetic nanoplatform or the GOQDs-coated magnetic nanoplatform. On the other hand, ELISA data clearly show that around 97% Hep G2 cells were captured when GOQDs were attached with an anti-GPC3 antibody. Our experimental results suggest that the HCC tumor cell capture efficiency using an anti-GPC3-antibody-attached GOQDs-decorated magnetic nanoplatform can be as high as 97%. The TEM image of captured Hep G2 cells, in Figure 3B, shows that GOQDs-decorated magnetic nanoplatforms are attached with tumor cells. For a comparison, we also performed TEM imaging for only Hep G2 cells, as reported in Figure 3C.

Because of the very high two-photon absorption cross section and good photostability and biocompatibility, we used anti-GPC3-antibody-attached GOQDs-decorated magnetic-nanoplatform-based two-photon imaging to visualize the capture Hep G2 cancer cells. Figure 3D shows the TPL image of Hep G2 tumor cells, which indicates that the multifunctional magnetic nanoplatform can be used for very bright two-photon imaging of cancer cells.

Parts E and F of Figure 3 show that the anti-GPC3-antibody-attached GOQDs-decorated magnetic nanoplatforms do not bind with blood cells; as a result, we have not observed any luminescence from the supernatant. To find out how selective the cell separation for Hep G2 tumor cells using anti-GPC3-antibody-attached GOQDs-decorated magnetic nanoplatforms is, we performed cell separation and two-photon imaging experiments using GPC3(−)−SK-BR-3 breast tumor cells. For this purpose, infected blood containing $3.5 \times 10^3$ SK-BR-3 tumor cells in 15 mL suspensions of citrated whole rabbit blood was incubated with 500 $\mu$L of the anti-GPC3-antibody-attached

GOQDs-coated magnetic nanoplatform for 90 min with gentle shaking. We used a bar magnet to separate cells attached to anti-GPC3-antibody-attached GOQDs-decorated magnetic nanoplatforms. Parts G and H of Figure 3 show that the anti-GPC3-antibody-attached GOQDs-decorated magnetic nanoplatforms do not bind with GPC3(−)−SK-BR-3 breast tumor cells. As a result, we have not observed any luminescence from the magnetic-separated portion. All of the above-reported experimental data clearly support that the anti-GPC3-antibody-attached GOQDs-decorated magnetic nanoplatform is highly selective for binding with the Hep G2 tumor cells, which overexpresses GPC3.

Because CTCs coexist with the peripheral blood mononuclear cells and other normal cells in an actual infected blood sample from patients, we performed experiments with the mixture of Hep G2 tumor cells and a normal-cell-infected blood sample. Citrated whole rabbit blood was infected by Hep G2 tumor cells, peripheral blood mononuclear cells (PBMCs), and HaCaT normal skin cells. Because the CTC concentration in blood is usually only around 10 cells/mL, in this experiment we kept the concentration of each cell after mixing so that the Hep G2 tumor cell concentration was only 10 cells/mL. In contrast, we kept the concentration of PBMC and HaCaT cells at $10^5$ cells/mL each in the infected blood sample. Figure 3I shows the ELISA data, which indicate that the Hep-G2 tumor cells capturing efficiency using our developed multifunctional anti-GPC3-antibody-attached GOQDs-decorated magnetic nanoplatform is about 91%, even in the presence of $10^4$ times more of PBMC and HaCaT cells each.

## 4. CONCLUSIONS

In conclusion, we reported the design and synthesis of multifunctional biocompatible anti-GPC3-antibody-attached GOQDs-decorated magnetic nanoplatforms that can deliver targeted capture of cancer cells from an infected blood sample, followed by accurate analysis using two-photon imaging. We showed that the multifunctional magnetic nanoplatform can be used for selective Hep G2 hepatocellular carcinoma tumor cell separation and enrichment from an infected blood sample. Reported TPL results indicated an extremely high two-photon absorption cross section (40530 GM) from the anti-GPC3-antibody-attached GOQDs-coated magnetic nanoplatform, which is about 3 orders of magnitude higher than well-studied organic dyes. Reported data indicated that the biocompatibility is very good for our design multifunctional material. Our experimental results showed that the biocompatibility was very good for the multifunctional nanoplatform. We also demonstrated that our designed multifunctional biocompatible-material-based TPL platform can be used for selective and very bright imaging of Hep G2 hepatocellular carcinoma tumor cells in biological transparency windows using 960 nm light. Experimental results with nontargeted GPC3(−)−SK-BR-3 breast cancer cells indicated that the anti-GPC3-antibody-attached GOQDs-decorated magnetic-nanoplatform-based cell separation from an infected blood sample followed by two-photon imaging was highly selective for Hep G2 hepatocellular carcinoma tumor cells. We also demonstrated that the capture efficiency was about 91% when a 15 mL infected blood sample containing 10 cells/mL Hep G2 tumor cells was used, which was relevant to the real-life clinical sample. Because of the very high TPL signal and good photostability, after proper engineering design, the multifunctional biocompatibility material is a good candidate for rare tumor cell separation and

two-photon cancer imaging in clinical settings. Although we performed CTC detection after separation from blood, it will be best for the clinical doctors to use real-time noninvasive imaging of CTCs as rare tumor cells flow through the peripheral vasculature. This can be done by injecting of a tumor-specific bioconjugated fluorescent ligand into the body, followed by multiphoton fluorescence imaging of superficial blood vessels. For this purpose, material reported by us will be the most useful.

## ■ AUTHOR INFORMATION

**Corresponding Author**
*E-mail:paresh.c.ray@jsums.edu. Fax: +16019793674.
**Notes**
The authors declare no competing financial interest.

## ■ ACKNOWLEDGMENTS

## ■ REFERENCES

(1) http://www.cancer.org/cancer/livercancer, date of access 03/02/2015.

(2) Qu, L.; Xu, J.; Tan, X.; Liu, Z.; Xu, L.; Peng, R. Dual-Aptamer Modification Generates a Unique Interface for Highly Sensitive and Specific Electrochemical Detection of Tumor Cells. *ACS Appl. Mater. Interfaces* **2014**, *6*, 7309−7315.

(3) Zhang, Y.; Li, J.; Cao, L.; Xu, W.; Yin, Z. Circulating Tumor Cells in Hepatocellular Carcinoma: Detection Techniques, Clinical Implications, and Future Perspectives. *Semin. Oncol.* **2012**, *39*, 449−460.

(4) Wu, L. J.; Pan, Y. D.; Pei, X. Y.; Chen, H.; Nguyen, S.; Kashyap, A.; Liu, J.; Wu, J. Capturing Circulating Tumor Cells of Hepatocellular Carcinoma. *Cancer Lett.* **2012**, *326*, 17−22.

(5) Xu, W.; Cao, L.; Chen, L.; Li, J.; Zhang, X. F.; Qian, H. H.; Kang, X. Y.; Zhang, Y.; Liao, J.; Shi, L. H.; Yang, Y. F.; Wu, M. C.; Yin, Z. F. Isolation of Circulating Tumor Cells in Patients with Hepatocellular Carcinoma Using a Novel Cell Separation Strategy. *Clin. Cancer Res.* **2011**, *17*, 3783−3793.

(6) Nellore, B. P. V.; Kanchanapally, R.; Pramanik, A.; Sinha, S. S.; Chavva, S. R.; Hamme, A.; Ray, P. C. Aptamer-Conjugated Graphene Oxide Membranes for Highly Efficient Capture and Accurate Identification of Multiple Types of Circulating Tumor Cells. *Bioconjugate Chem.* **2015**, *26*, 235−242.

(7) Chaffer, C. L.; Weinberg, R. A. A Perspective on Cancer Cell Metastasis. *Science* **2011**, *331*, 1559−1564.

(8) Wang, S.; Liu, K.; Liu, J.; Yu, Z. T. F.; Xu, X.; Zhao, L.; Lee, T.; Lee, E. K.; Reiss, J.; Lee, Y.-K.; Chung, L. W. K.; Huang, J.; Rettig, M.; Seligson, D.; Duraiswamy, K. N.; Shen, C. K. F.; Tseng, H.-R. Highly Efficient Capture of Circulating Tumor Cells by Using Nanostructured Silicon Substrates with Integrated Chaotic Micromixers. *Angew. Chem., Int. Ed.* **2011**, *50*, 3084−3088.

(9) Yu, M.; Bardia, A.; Aceto, N.; Bersani, F.; Madden, M. W.; Donaldson, M. C.; Desai, R.; Zhu, H.; Comaills, V.; Zheng, Z.; Wittner, B. S.; Stojanov, P.; Brachtel, E.; Sgroi, D.; Kapur, R.; Shioda, T.; Ting, D. T.; Ramaswamy, S.; Getz, G.; Iafrate, A. J.; Benes, C.; Toner, M.; Maheswaran, S.; Haber, D. A. A. Cancer Therapy. Ex Vivo Culture of Circulating Breast Tumor Cells for Individualized Testing of Drug Susceptibility. *Science* **2014**, *345*, 216−220.

(10) Lohr, J. G.; Adalsteinsson, V. A.; Cibulskis, K.; Choudhury, A. D.; Rosenberg, M.; Cruz-Gordillo, P.; Francis, J. M.; Zhang, C. Z.; Shalek, A. K.; Satija, R.; Trombetta, J. J.; Lu, D.; Tallapragada, N.; Tahirova, N.; Kim, S.; Blumenstiel, B.; Sougnez, C.; Lowe, A.; Wong, B.; Auclair, D.; Van Allen, E. M.; Nakabayashi, M.; Lis, R. T.; Lee, G.

S.; Li, T.; Chabot, M. S.; Ly, A.; Taplin, M. E.; Clancy, T. E.; Loda, M.; Regev, A.; Meyerson, M.; Hahn, W. C.; Kantoff, P. W.; Golub, T. R.; Getz, G.; Boehm, J. S.; Love, J. C. Whole-Exome Sequencing of Circulating Tumor Cells Provides a Window into Metastatic Prostate Cancer. *Nat. Biotechnol.* **2014**, *32*, 479−484.

(11) Yoon, H. J.; Kozminsky, M.; Nagrath, S. Emerging Role of Nanomaterials in Circulating Tumor Cell Isolation and Analysis. *ACS Nano* **2014**, *8*, 1995−2017.

(12) Wang, S.; Liu, K.; Liu, J.; Yu, Z. T. F.; Xu, X.; Zhao, L.; Lee, T.; Lee, E. K.; Reiss, J.; Lee, Y.-K.; Chung, L. W. K.; Huang, J.; Rettig, M.; Seligson, D.; Duraiswamy, K. N.; Shen, C. K. F.; Tseng, H.-R Highly Efficient Capture of Circulating Tumor Cells by Using Nanostructured Silicon Substrates with Integrated Chaotic Micromixers. *Angew. Chem., Int. Ed.* **2011**, *50*, 3084−3088.

(13) Fan, Z.; Senapati, D.; Singh, A. K.; Ray, P. C. Theranostic Magnetic Core−Plasmonic Shell Star Shape Nanoplatform for the Isolation of Targeted Rare Tumor Cells from Whole Blood, Fluorescence Imaging, and Photothermal Destruction of Cancer. *Mol. Pharmaceutics* **2013**, *10*, 857−866.

(14) Fan, Z.; Shelton, M.; Singh, A. K.; Senapati, D.; Khan, S. A.; Ray, P. C. Multifunctional Plasmonic Shell−Magnetic Core Nanoplatforms for Targeted Diagnostics, Isolation, and Photothermal Destruction of Tumor Cells. *ACS Nano* **2012**, *6*, 1075−1083.

(15) Liu, X.; Wang, S. Three-Dimensional Nano-Biointerface as a New Platform for Guiding Cell Fate. *Chem. Soc. Rev.* **2014**, *43*, 2385−2401.

(16) Yoon, H. J.; Kim, T. H.; Zhang, Z.; Azizi, E.; Pham, T. M.; Paoletti, C.; Lin, J.; Ramnath, N.; Wicha, M. S.; Hayes, D. F.; Simeone, D. M.; Nagrath, S. Sensitive Capture of Circulating Tumour Cells by Functionalized Graphene Oxide Nanosheets. *Nat. Nanotechnol.* **2013**, *8*, 735−741.

(17) Geim, A. K.; Novoselov, K. S. The Rise of Graphene. *Nat. Mater.* **2007**, *6*, 183−191.

(18) Chou, S. S.; De, M.; Luo, J.; Rotello, V. M.; Huang, J.; Dravid, V. P. Nanoscale Graphene Oxide (nGO) as Artificial Receptors: Implications for Biomolecular Interactions and Sensing. *J. Am. Chem. Soc.* **2012**, *134*, 16725−16733.

(19) Hummers, W. S.; Offeman, R. E. Preparation of Graphitic Oxide. *J. Am. Chem. Soc.* **1958**, *80*, 1339−133.

(20) Fan, Z.; Kanchanapally, R.; Ray, P. C. Hybrid Graphene Oxide Based Ultrasensitive SERS Probe for Label-Free Biosensing. *J. Phys. Chem. Lett.* **2013**, *4*, 3813−3818.

(21) Pramanik, A.; Chavva, S. R.; Fan, Z.; Sinha, S.; Nellore, B. P.; Ray, P. C. Extremely High Two-Photon Absorbing Graphene Oxide for Imaging of Tumor Cells in the Second Biological Window. *J. Phys. Chem. Lett.* **2014**, *5*, 2150−2154.

(22) Pramanik, A.; Fan, Z.; Reddy S. C.; Sinha, S. S.; Ray, P. C. Highly Efficient and Excitation Tunable Two-Photon Luminescence Platform For Targeted Multi-Color MDRB Imaging Using Graphene Oxide. *Sci. Rep.* **2014**, *4*, Article No. 6090.

(23) Kamat, P. V. Graphene-Based Nanoarchitectures. Anchoring Semiconductor and Metal Nanoplatforms on a Two-Dimensional Carbon Support. *J. Phys. Chem. Lett.* **2014**, *1*, 520−527.

(24) Fan, Z.; Yust, B.; Nellore, B. O. V; Sinha, S. S.; Kanchanapally, R.; Crouch, R. A.; Pramanik, A.; Reddy, S. C.; Sardar, D.; Ray, P. C. Accurate Identification and Selective Removal of Rotavirus Using a Plasmonic−Magnetic 3D Graphene Oxide Architecture. *J. Phys. Chem. Lett.* **2014**, *5*, 3216−3221.

(25) Pan, D.; Zhang, J.; Li, Z.; Wu, M. Hydrothermal Route for Cutting Graphene Sheets into Blue Luminescent Graphene Quantum Dots. *Adv. Mater.* **2010**, *22*, 734−738.

(26) Lu, J.; Yeo, P. S. E.; Gan, C. K.; Wu, P.; Loh, K. P. Transforming C60 Molecules into Graphene Quantum Dots. *Nat. Nanotechnol.* **2011**, *6*, 247−252.

(27) Moon, J. H.; An, J. H.; Sim, U.; Cho, S. P.; Kang, J. H.; Chung, C.; Seo, J. H.; Lee, J. H.; Nam, K. T.; Hong, B. H. One-Step Synthesis of N-Doped Graphene Quantum Sheets from Monolayer Graphene by Nitrogen Plasma. *Adv. Mater.* **2014**, *26*, 3501−3505.

(28) Yan, X.; Cui, X.; Li, L. S. Synthesis of Large, Stable Colloidal Graphene Quantum Dots with Tunable Size. *J. Am. Chem. Soc.* **2010**, *132*, 5944−5945.

(29) Peng, J.; Gao, W.; Gupta, B. K.; Liu, Z.; Romero-Aburto, R.; Ge, L.; Ajayan, P. M. Graphene Quantum Dots Derived from Carbon Fibers. *Nano Lett.* **2012**, *12*, 844−849.

(30) Lin, S. H.; Kim, D. H.; Jun, G. H.; Hong, S. H.; Jeon, S. Tuning the Photoluminescence of Graphene Quantum Dots through the Charge Transfer Effect of Functional Groups. *ACS Nano* **2013**, *7*, 1239−1245.

(31) Mueller, M. L.; Yan, X.; McGuire, J. A.; Li, L. Triplet States and Electronic Relaxation in Photoexcited Graphene Quantum Dots. *Nano Lett.* **2010**, *10*, 2679−2682.

(32) Dong, Y. Q.; Pang, H. C.; Yang, H. B.; Guo, C. X.; Shao, J. W.; Chi, Y. W.; Li, C. M.; Yu, T. Carbon-Based Dots Co-Doped with Nitrogen and Sulfur for High Quantum Yield and Excitation-Independent Emission. *Angew. Chem., Int. Ed.* **2013**, *52*, 7800−7804.

(33) Baker, S. N.; Baker, G. A. Luminescent Carbon Nanodots: Emergent Nanolights. *Angew. Chem., Int. Ed.* **2010**, *49*, 6726−6744.

(34) Li, Y.; Zhao, Y.; Cheng, H.; Hu, Y.; Shi, G.; Dai, L.; Qu, L. Nitrogen-Doped Graphene Quantum Dots with Oxygen-Rich Functional Groups. *J. Am. Chem. Soc.* **2011**, *134*, 15−18.

(35) Yan, X.; Li, B.; Cui, X.; Wei, Q.; Tajima, K.; Li, L. Independent Tuning of the Band Gap and Redox Potential of Graphene Quantum Dots. *J. Phys. Chem. Lett.* **2011**, *2*, 1119−1124.

(36) Pan, D.; Zhang, J.; Li, Z.; Wu, M. Hydrothermal Route for Cutting Graphene Sheets into Blue-Luminescent Graphene Quantum Dots. *Adv. Mater.* **2010**, *22*, 734−738.

(37) Li, L.-S.; Yan, X. Colloidal Graphene Quantum Dots. *J. Phys. Chem. Lett.* **2010**, *1*, 2572−2576.

(38) Lhien, C.; Li, S.; Lai, W.; Yeh, Y.; Chen, H.; Chen, I.; Chen, L.; Chen, K.; Nemoto, T.; Isoda, S.; Chen, M.; Fujita, T.; Eda, G.; Yamaguchi, H.; Chhowlla, M.; Chen, C. Tunable Photoluminescence from Graphene Oxide. *Angew. Chem., Int. Ed.* **2012**, *51*, 6662−6666.

(39) Song, Y.; Pang, H.; Yang, H. B.; Guo, C.; Shao, J.; Chi, Y.; Li, C. M.; Yu, T. Carbon-based Dots Co-doped with Nitrogen and Sulfur for High Quantum Yield and Excitation-Independent Emission. *Angew. Chem., Int. Ed.* **2013**, *52*, 7800−7804.

(40) Liu, Q.; Guo, B.; Rao, Z.; Zhang, B.; Gong, J. R. Strong Two-Photon-Induced Fluorescence from Photostable, Biocompatible Nitrogen-Doped Graphene Quantum Dots for Cellular and Deep-tissue Imaging. *Nano Lett.* **2013**, *13*, 2436−2441.

(41) Wang, L.; Zhu, S.-J.; Wang, H.-Y.; Qu, S.-N.; Zhang, Y.-L.; Zhang, J.-H.; Chen, Q.-D.; Xu, H.-L.; Han, W.; Yang, B.; Sun, H.-B. Common Origin of Green Luminescence in Carbon Nanodots and Graphene Quantum Dots. *ACS Nano* **2014**, *8*, 2541−2547.

(42) Li, J.-L.; Bao, H.-C.; Hou, X.-L.; Sun, L.; Wang, X.-G.; Gu, M. Graphene Oxide Nanoplatforms as a Nonbleaching Optical Probe for Two-Photon Luminescence Imaging and Cell Therapy. *Angew. Chem., Int. Ed.* **2012**, *51*, 1830−1834.

(43) Demeritte, T.; Fan, Z.; Sinha, S. S.; Duan, J.; Pachter, R.; Ray, P. C. Gold Nanocage Assembly for Selective Second Harmonic Generation Imaging of Cancer Cell. *Chem.—Eur. J.* **2014**, *20*, 1017−1022.